Plasma Medicine, 15(1):33–52 (2025)

Mercury-Free Lamp-Phosphor Coupling for UVC Surface Decontamination

Abdoul Baraze,[a,b,*] Cristina Muja,[a] Ibtissam Courti,[a] Florent P. Sainct,[a] Sébastien Allix,[b] Philippe Guillot,[a] & Thomas Maho[a]

[a]Laboratoire DPHE, Université de Toulouse, INU Champollion, Place de Verdun, Albi, France; [b]Lab'Science, Boulevard de l'Industrie, Nazelles-Négron, France

*Address all correspondence to: Thomas Maho, Laboratoire DPHE, Université de Toulouse, INU Champollion, Place de Verdun, 81000 Albi, France; Tel.: +33 5 63 48 64 31, E-mail: thomas.maho@univ-jfc.fr

ABSTRACT: Microbiological contamination of surfaces is a significant issue across various sectors, posing a serious risk of pathogen transmission between individuals and impacting public health. Among the available decontamination methods, ultraviolet-C (UVC) radiation has seen a surge in popularity in recent years, particularly following the COVID-19 pandemic. However, concerns have been raised regarding the environmental impact and the risk for users of mercury-containing UVC devices. Despite their well-documented biocidal efficacy against a broad spectrum of microorganisms, UVC radiation can be significantly hindered by the presence of organic matter, biofilms, or surface irregularities that create shadowed areas. In this study, we present an innovative approach that combines a krypton-chlorine (KrCl) excimer lamp with a UVC phosphor. Optical characterization techniques—including optical emission spectroscopy, camera imaging, and irradiance measurements—were used to analyze the KrCl lamp and two lamp-phosphor combinations, revealing the complementary nature of these two UVC sources. This synergy was further investigated and validated against two bacterial species (*Escherichia coli* and *Staphylococcus aureus*) and the HAdV5 adenovirus. The promising results highlight new opportunities for enhancing UVC-based surface decontamination strategies by combining UVC radiation sources.

KEY WORDS: mercury-free lamp, far-UVC, phosphor, plasma, decontamination, irradiation, microbiology, virology

I. INTRODUCTION

Microbiological contamination of surfaces is a significant issue across various sectors, including the food industry,[1–3] public spaces,[4] hospitals, and other healthcare facilities.[5,6] Studies have demonstrated that bacteria,[7] viruses,[8] and fungi[9] can persist on dry inanimate surfaces for extended periods, sometimes for months, with increased survival under humid and low-temperature conditions. Maintaining surface cleanliness is therefore essential to controlling pathogen transmission.

Conventional surface decontamination methods include chemical or physical approaches. Chemical disinfectants, such as alcohol-based solutions, quaternary ammonium compounds, chlorine, and hydrogen peroxide are commonly used to eliminate or reduce microbial presence.[10] They have a broad spectrum of antimicrobial activity and act on several targets in microbial cells.[11] However, the effectiveness of

1947-5764/25/$35.00

decontamination procedures is influenced by several factors, including frequency, methodology, equipment, monitoring protocols, and surface cleanliness standards.[12,13] Certain microorganisms exhibit resistance to specific chemical agents, either intrinsically, through acquired resistance, or by being shielded within biofilms.[14–16] The use of chemical products can lead to the generation of toxic residues, the degradation of sensitive materials, and an increase of the emergence of multiresistant microorganisms.[17,18] For these reasons, chemical-free methods should be favored wherever possible.

Physical methods include radiation, dry-ice cleaning, ice-pigging, and ultrasound.[19] Among these methods, ultraviolet (UV) light (200–400 nm) has been used for many years to disinfect contaminated surfaces due to their germicidal properties.[20] When interacting with microorganisms, ultraviolet-C (UVC) (200–280 nm) radiation induces irreversible damage to their deoxyribonucleic acid (DNA) or ribonucleic acid (RNA) by forming pyrimidine dimers, which disrupt replication and transcription of the DNA.[21] Historically, low-pressure mercury vapor lamps have been widely used to generate UVC radiation, with a dominant emission at 254 nm. These devices operate via electrical discharge in a plasma with mercury amalgam, where electrons excite mercury atoms to emit ultraviolet photons. Although these lamps are effective and well-established, the presence of mercury (which raises environmental concerns), their limited lifespan and mechanical fragility further constrain their use.[22,23] Moreover, 254 nm UVC is considered to be hazardous to human health as it is a potential cause of dermatitis and skin cancer.[24,25]

In an attempt to reduce the hazardous effects of conventional mercury lamp, researchers focused on excimer lamps.[26] These devices operate based on the principle of dielectric barrier discharges (DBDs), in which a rare gas (such as krypton or xenon) is excited in the presence of halogens (chlore, brome, iode, as examples) to form ephemeral molecules called excimers.[27] These unstable molecules dissociate, emitting characteristic UV radiation. For example, the excimer molecule krypton-chlorine (KrCl) predominantly emits at a wavelength of 222 nm, within the germicidal range of UVC.[28] It has been shown that 222 nm is harmless to mammalian cells, human skin, and eyes when applied at controlled intensities.[29,30] When coupled with phosphors, excimer lamps can extend their emission spectrum or enhance their germicidal efficiency.[31] Phosphors convert part of the energy emitted by the excimer into a different UVC wavelength optimized for microorganism inactivation.[32,33]

The use of UVs has the advantage of being both rapid and effective in inactivating a wide range of microorganisms, including viruses, bacteria, and spores.[34] However, the effectiveness of UVC light can be influenced by several factors, such as the presence of organic matter, surface texture, and the uniformity of exposure. To overcome these limitations and to target microorganisms that may exhibit reduced sensitivity to a single wavelength, we propose an innovative mercury-free hybrid approach that combines a KrCl excimer lamp with a phosphor, both emitting in the UVC range.

II. MATERIALS AND METHODS

A. Experimental Setup

1. Principle

The system comprises a support material, a phosphor powder, a quartz plate, and a light source positioned horizontal to the surface (Fig. 1). When the phosphor is excited by the light source (named R_{LAMP}), it emits radiation (noted $R_{PHOSPHOR}$). Outside of this situation, the powder does not emit any light. The innovation of the system lies in the complementary interaction between the two radiations, $R_{PHOSPHOR}$ and R_{LAMP}. When both are emitted, resulting in $R_{COMBINED}$, microorganisms present on the glass surface are effectively sandwiched between two UVC rays, creating a biocidal synergy.[35]

a. Phosphor's Characteristics

The phosphor used is a calcium pyrophosphate ($Ca_2P_2O_7$) doped with Pr^{3+} ions. These characteristics are detailed in our previous study.[33] In this work, the phosphor powder was synthesized using spray pyrolysis (SP) at the CEMES laboratory[32] or solid-state reaction (SSR) by Phosphor Technology. The resulting powders SP and SSR were then deposited onto a quartz substrate using the sol-gel technique.[36] This process involves incorporating the phosphor into a chemical solution containing a metal precursor (tetraethyl orthosilicate), an acid catalyst (chloride acid, HCl), and water (H_2O) to create a sol. Over time, the sol particles assemble into a three-dimensional solid network, forming a gel. The gel is air-dried on the quartz plate until it solidifies.

b. UVC Light Source's Characteristics

The light source is a plasma lamp designed by OLISCIE and operating on the principle of a coaxial DBD (Fig. 2). It consists of an inner glass tube with a diameter of 15 mm into which a high-voltage electrode is inserted, and an outer glass tube with a diameter

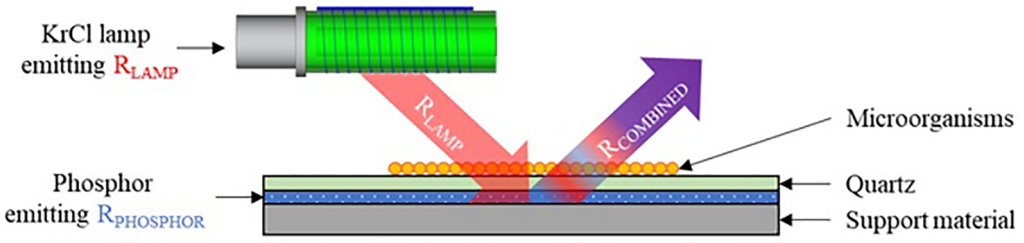

FIG. 1: Schematic of the experimental setup. The light emitted by the lamp and the phosphor are R_{LAMP} and $R_{PHOSPHOR}$, respectively. $R_{COMBINED}$ is the combination of $R_{LAMP} + R_{PHOSPHOR}$.

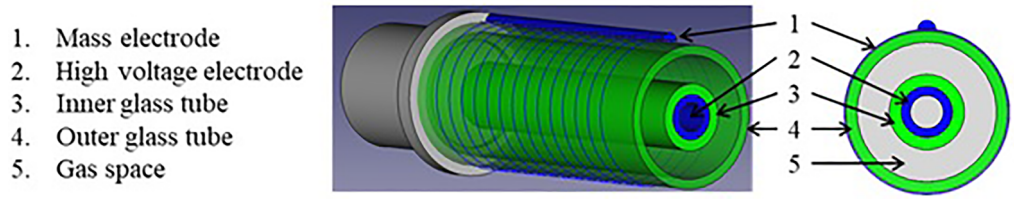

FIG. 2: Schematic of the KrCl excimer lamp

of 50 mm around which metal cable is wrapped to act as a ground electrode. The two tubes form a hermetically sealed glass chamber measuring 200 mm in length. This enclosure contains a mixture of KrCl gas at a pressure of between 200 and 400 mbar.

The lamp is powered by a voltage-limited pulse generator, also developed by OLISCIE. The voltage is fixed at 3.5 kV, while the current is adjustable from 1 to 10 A to deliver the required control power, ranging from 10 to 100 W, over a frequency range of 20–100 kHz. The characteristic voltage and current signals from the power supply are shown in Fig. 3. The current pulse duration is 1.5 µs. These signals were observed using an oscilloscope (Rodhe & Schwarz RTE1024) equipped with a high-voltage probe (Tektronix P6015A) and a current probe (Pearson™ current monitor, model 6585).

B. UVC Source Characterization

1. Irradiance Measurement

The radiation power received per unit area on the surface was measured using a radiometer (RM-12 UVC, Optysec Dr. Gröbel). The device detects wavelengths in the range

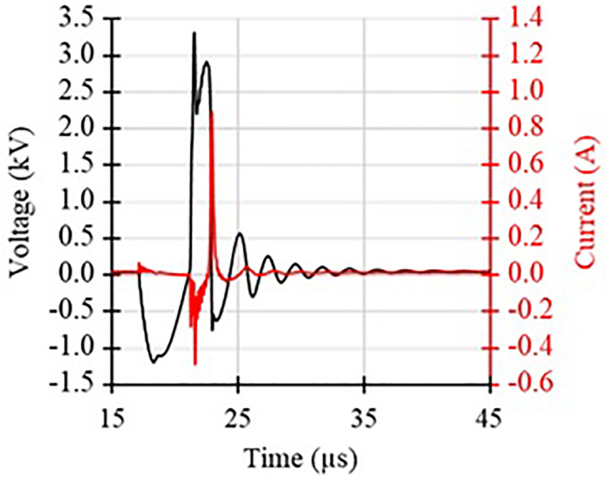

FIG. 3: Voltage and current signals delivered by the pulse generator

of 200–280 nm and provides irradiance measurements from 0 to 199 mW/cm², with a resolution of 0.01 mW/cm². The radiometer was calibrated by the manufacturer at 222 nm using a krypton-chlorine excimer lamp (Heraeus) and at 254 nm using a mercury lamp (TÜV, model 15W/G15 T8).

2. Optical Emission Spectroscopy

The radiation emitted by the KrCl lamp and the irradiated phosphors were studied with a SpectraPro PI-HRS-750 monochromator equipped with a 300 tr/mm grating. The light was collected using a 600 µm diameter QP6000-2-SR optical fiber and then detected at the spectrometer's output by an ICCD camera Pi-Max-4.

3. Camera Imaging

The distribution of streamers produced in the plasma discharge was observed with an intensified charge-coupled device (ICCD) camera Pi-Max-2K-RB having a resolution of 1,024 × 1,204 pixels. The red-blue (RB) intensifier enables a wavelength range measurable by the camera between 200 and 900 nm. The CCD matrix is Peltier-cooled down to –20°C to reduce dark current, thus improving the signal-to-noise ratio.

4. Bactericidal Efficacy Assessment and Morphological Analysis of Bacterial Cells

Escherichia coli ATCC 47076 and *Staphylococcus aureus* ATCC 6538 were used in this study as model microorganisms for Gram negative and Gram positive bacteria. The assessment of the bactericidal efficacy was made according to NF EN 17272 with slight modifications. Briefly, both strains were grown on tryptic soy agar plates at 37°C overnight, and bacterial suspensions in sterile phosphate buffered were obtained and adjusted at 4.0×10^8 CFU/ml. The suspension (50 µl) was spread on the surface of these natural quartz plates (20 × 20 × 0.5 mm) and allowed to dry. The contaminated samples were then exposed to a lamp operating at a power of 20 W for 5, 10, 20, 30, and 60 s, with a fixed lamp to surface distance of 10 cm. The radiation emitted by the lamp at this distance was 0.58 mW/cm². Following the exposure period, the quartz plate was transferred into a tube with sterile diluent. Subsequently, a serial dilution was performed up to 10^5, and trypticase soy agar (TSA) plates were inoculated with 0.1 ml of each dilution in triplicate, followed by incubation at 37°C over a duration of 48 hr. To assess the viability of microorganisms within the rest of the bacterial suspension, the membrane filtration technique was employed. The remaining sample was filtered through a membrane with a pore size of 0.45 mm, and the membranes were placed on TSA plates for incubation. Visible colonies that developed were enumerated at intervals of 24 and 48 hr. The results were documented as colony-forming units (CFUs) and computed for each sample (CFU/sample).

The effect of UV treatment on the bacterial morphology was investigated by scanning electron microscopy (SEM). *E. coli* or *S. aureus* contaminated quartz samples

(5 × 5 × 0.5 mm) were prepared and treated as described earlier. Following UV exposure, the carriers were immersed in 2.5% glutaraldehyde and kept for 24 hr at 4°C. After that, the samples were washed from fixative, routinely dehydrated in ethanol, and sputtered with platinum using a high vacuum coating system (Leica EM MED 020). The samples were imaged in a Quanta 250 FEG scanning electron microscope under high vacuum at 10.00 kV, and SEM images were recorded with magnifications from 3,000× to 35,000×. Untreated samples were processed in the same manner and used as controls. Post-treatment sample preparation and imaging were made at the Centre de Microscopie Électronique (CMEAB, Université de Toulouse III-Paul Sabatier, Toulouse, France).

5. Virucidal Efficacy Assessment

The virucidal efficacy was investigated by a focus-forming assay using human adenovirus HAdV-5 ANCHOR™ (4.10^7 FFU/ml) as model virus. Viral stock suspension (10 µl) was spread on a 1 × 1 cm quartz coverslip. After drying for 10–15 min, samples were subjected to one of three conditions: left in the dark, irradiated with the KrCl lamp, or irradiated with the KrCl lamp on a surface. The KrCl lamp was activated for 60 s at 20 W, positioned 10 cm from the sample, delivering an exposure dose of 34.8 mJ/cm^2. Treated quartz coverslips were transferred to 35 mm Petri dishes, and the virus was recovered by washing twice with 200 µl cell media. After treatment, 100 µl of the viral suspension was used to infect HEK393 cells (plated at 11×10^3 cells/well the day before the experiment) in a 96-well plate. Serial ten-fold dilutions of the suspension were prepared, and the lowest dilution with infected cells was recorded. At 24 hr post-infection, cells were fixed with formalin and stained with Hoechst 33342 to visualize nuclei. Images were acquired and analyzed using a Thermo CellInsight CX7 high-content microscope. These experiments were conducted in collaboration with NeoVirTech, Toulouse, France.

III. RESULTS

A. Plasma Lamp's Characteristics

In the literature, it is well known that for rare gas halogen exciplex molecules, the B–X transition is the highest in intensity, but there are also the weaker D–X, D–A, and C–A transitions, and emission bands of halogen dimer molecules.[37] A typical spectrum in the range from 200 to 400 nm of our discharge obtained in the KrCl lamp at 20W is shown in Fig. 4(a). The highest line corresponds to the $B_{1/2} \rightarrow X_{1/2}$ transition of the KrCl* exciplex at 222 nm. The emission of ~ 235 nm is due to the overlapping $C_{3/2} \rightarrow A_{3/2}$ and $D_{1/2} \rightarrow A_{1/2}$ transitions. Also present are the Cl_2* line at 259 nm and a broad, low-intensity emission near 325 nm due to the trimer emission Kr_2Cl*.[38]

One advantage of excilamps is that up to 80% of the total radiant flux can be concentrated in a relatively narrow emission band, at 222 nm in the case of KrCl.[39] Another advantage of excilamp is the independence of the discharge ignition on the temperature of their operating media and the short time of the discharge ignition. As depicted in

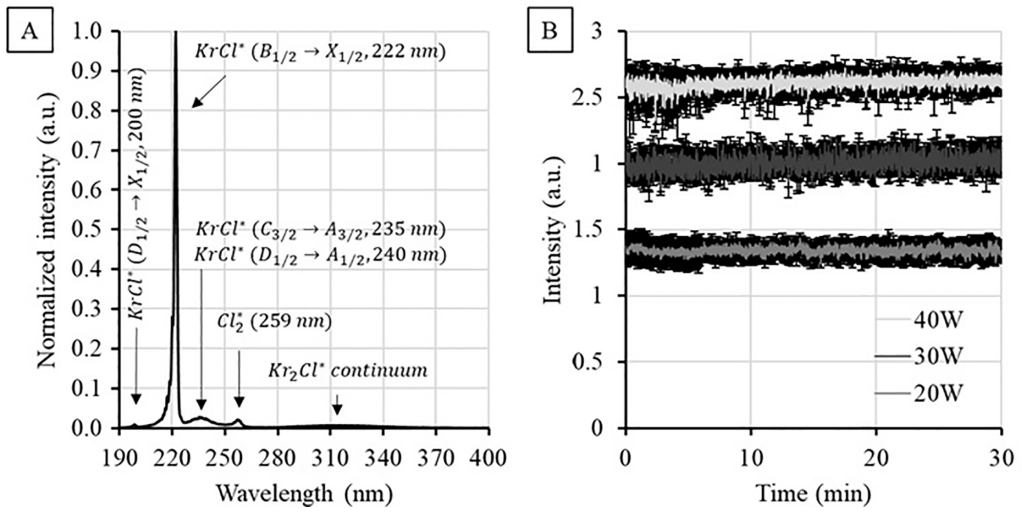

FIG. 4: (a) Optical spectrum of the KrCl excimer lamp, considering as R_{LAMP}, and (b) evolution of the 222 nm KrCl line as function of time and power

Fig. 4(b), the lamp reaches a near-stationary operating mode very quickly, in about 0.5–1 s.[37] The UV intensity of the 222 nm emission generated by our KrCl excimer lamp becomes stable as soon as the lamp is switched on. The intensity increases by 49.2 and 94.4% when the power is increased from 20 to 30 W and from 20 to 40 W, respectively. Each curve represents the mean of three experiments, with error bars indicating the standard deviation.

Figure 5(a) was taken with a conventional camera to better appreciate the color of the discharge and its filamentary structure, whereas Fig. 5(b)–5(d) were recorded with an ICCD camera when the plasma discharge was generated with a power of 20, 30, and 40 W. The discharge is characterized by micro-discharges chaotically distributed in the discharge gap. Their formation steps are described by Lomaev et al.[40] The filament structure is due to the operating pressure, electrode configuration, the gases ratio, and the electrical parameters (frequency, waveform, pulse rate).[28] A capacitive discharge, operating at lower pressures (≤ 10 mbar), compared to the DBD-type discharge used here (a few hundred millibar), would produce a homogeneous discharge, but it would yield a less intense emission line at 222 nm.[41] This was also the conclusion reached by the work of Lomaev et al.,[40] who showed that the presence of filaments in the barrier discharge was the necessary condition for high-efficiency operation of a KrCl discharge lamp, because a uniform discharge distribution led to a reduction in radiation efficiency.[28,37,40]

The maps in Fig. 6 illustrate the irradiance measurements recorded over a 1,200 cm^2 surface exposed to the KrCl lamp, with control power set to Fig. 6(a) 20, 6(b) 30, and 6(c) 40 W. The distance between the KrCl lamp and the irradiance meter detector was 5 cm. Distinct zones were defined based on the irradiance values, ranging from 0.3

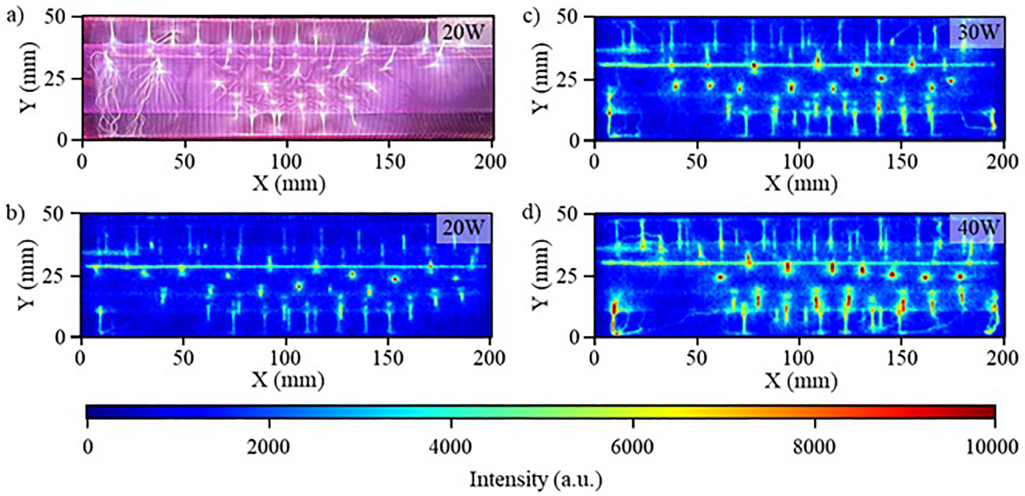

FIG. 5: (a) Photography and ICCD images of the KrCl excimer lamp working at (b) 20 W, (c) 30 W and (d) 40 W with an integration time of 400 µs

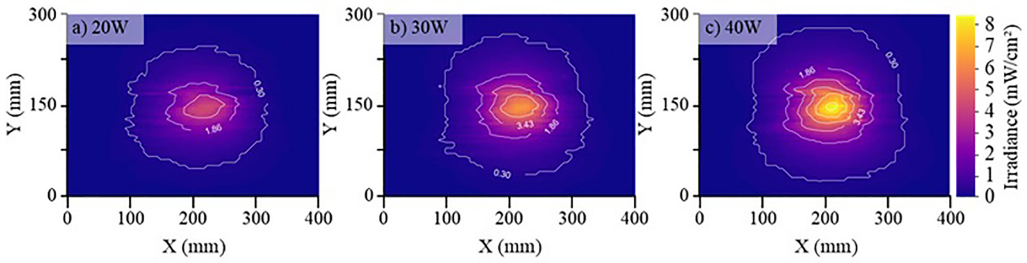

FIG. 6: Irradiance received by a surface of 12×10^2 cm² exposed to the KrCl excimer lamp powered at (a) 20, (b) 30, and (c) 40 W

to 6.55 mW/cm². The maps reveal a Gaussian distribution and an expansion of the areas receiving a given irradiance with increasing power. For instance, the area receiving at least 0.3 mW/cm² covers 465, 573, and 662 cm² at 20, 30, and 40 W, respectively. This corresponds to an increase of 23% between 20 and 30 W, and 43% between 20 and 40 W.

B. Phosphors Emission's Characteristics

In this section, the radiation emitted by the lamp will be referred to as R_{LAMP} and that of the phosphors as $R_{PHOSPHOR}$. The SP phosphor corresponds to the powder produced by SP using the CEMES laboratory protocol, while the "SSR" phosphor is produced by phosphor technology using the solid-state reaction method.

1. Measurement in Transmission

Figure 7 shows the emission spectra between 190 and 450 nm of the SP and SSR luminophores under excitation at 222 nm with a control power of 40 W [Fig. 7(a)]. They were obtained by filling a cylinder (Ø = 5 mm, thk = 1 mm) placed between two quartz plates with raw power [Fig. 7(b)]. The KrCl lamp and an optical fiber connected to a monochromator Pi-HRS-750 (grating 300 g/mm) were placed on either side of the quartz plates for measuring the radiation transmitted through the raw powder. In these conditions, we assume that the radiation detected in transmission comes exclusively from the luminophore, $R_{PHOSPHOR}$, with the powder absorbing 100% of the lamp's emission.

The characteristic emissions of the Pr^{3+} ion at 236.5, 251.7, 274.8, 336.5, and 416.5 nm originate from transitions between the $^1S_0$ level and the $^3H_6$, $^3F_4$, $^1G_4$, $^1D_2$, and $^1I_6$ levels, respectively. The processes (quantum splitting phosphor versus photon cascade emission) and conditions (such as energy, temperature, and pressure) for obtaining and promoting these transitions are detailed in Srivastava's studies.[42–45] These factors are primarily influenced by the composition and crystalline structure of the host matrices incorporating the Pr^{3+} ion. In our previous work,[33] we showed, in fact, that the Pr^{3+} emission intensity was much lower in $Sr_2P_2O_7$ and $LaPO_4$ than $Ca_2P_2O_7$ under vacuum ultraviolet excitation.

From transmission measurements, the spectral intensities were integrated over defined wavelength intervals to quantitatively assess the distribution of UV emissions (200–400 nm) across the UVC (200–280 nm), UVB (280–320 nm), and UVA (320–400 nm) spectral regions. The results presented in Fig. 8 reveal a more balanced distribution between UVC and UVB for the SP luminophore (13 and 16%, respectively) compared to the SSR luminophore (8 and 23%, respectively). Additionally, it is evident that both phosphors primarily emit within the UVA range. When comparing the total intensities of the SSR and SP powders, it is observed that the SP powder enables stronger emissions with +71% in the UVC range and +12% in the UVA range.

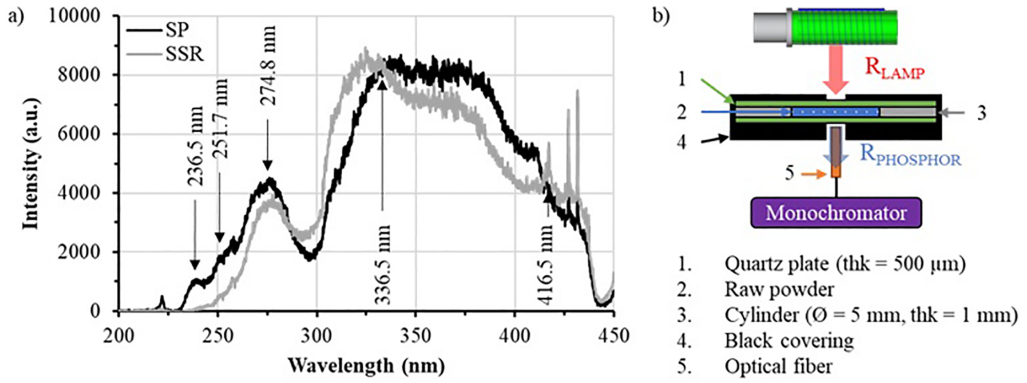

FIG. 7: (a) Optical spectrum of $R_{PHOSPHOR}$, SP and SSR, measured in transmission, after being excited with the KrCl excimer lamp working at 40 W. (b) Experimental set-up for the measurement in transmission.

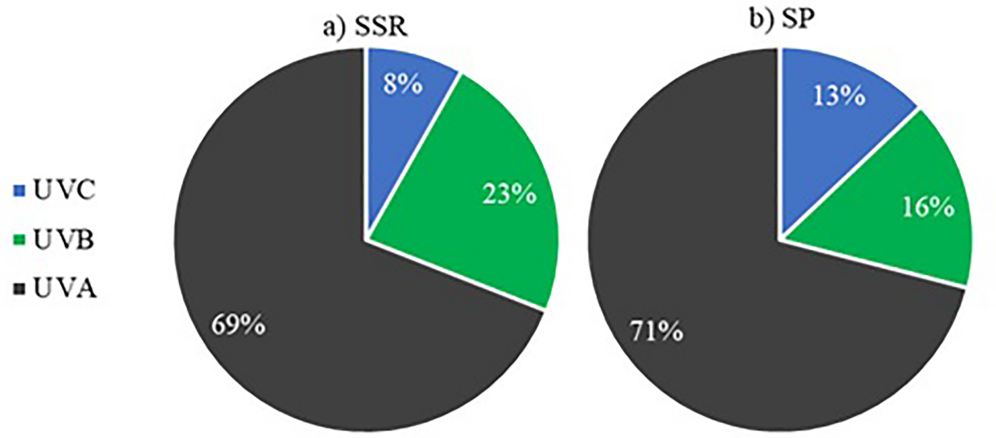

FIG. 8: Distribution (measured in percent) of radiation emitted by SSR and SP phosphors in the UVC (200–280 nm), UVB (280–320 nm), and UVA (320–400 nm) ranges, measured in transmission

2. Measurement in Reflection

In [Fig. 9(a)], the black spectrum corresponds to the reflection of the excitation radiation, R_{LAMP}, emitted by the KrCl lamp on a raw quartz plate without any phosphor deposition. A black paper was placed between the quartz and the support material to

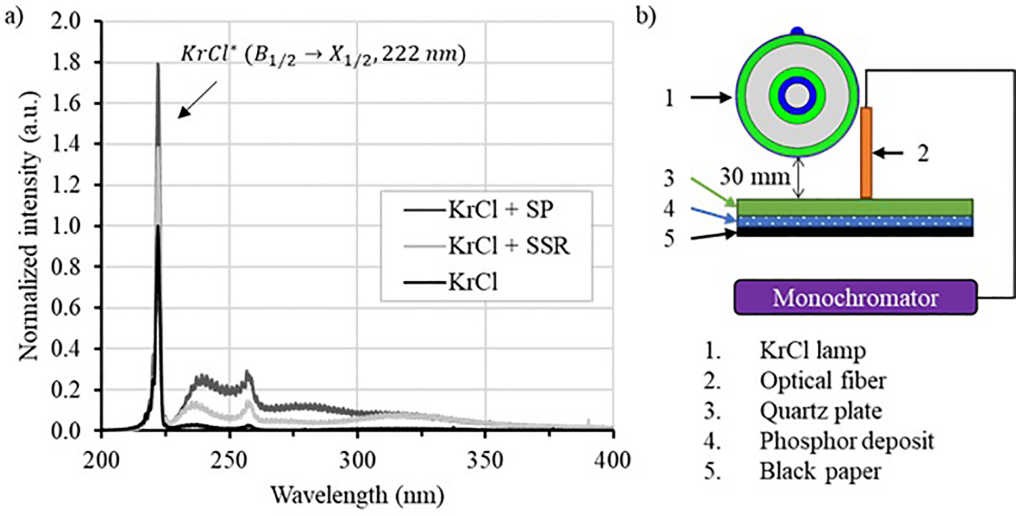

FIG. 9: (a) Optical spectrum of $R_{COMBINED}$, KrCl+SP and KrCl+SSR, measured in reflection, after being excited with the KrCl excimer lamp. All spectra are normalized to the maximal intensity of the KrCl excimer lamp. (b) Experimental set-up for the measurement in reflection.

avoid the reflection of the radiation emitted by the lamp on the support material. The gray and black spectra are the combination of the R_{LAMP} and the emission radiation, $R_{PHOSPHOR}$, from the SSR and SP phosphors, respectively. All the spectra are normalized to the maximal intensity measured for R_{LAMP}. In this experimental setup, the optical fiber body was positioned as close as possible to the lamp and directed toward the surface [Fig. 9(b)]. The lamp was placed 30 mm above the surface, while the entry of the fiber was positioned 2 mm above the surface. The shadow produced by the tip of the fiber was considered negligible. Under these conditions, the reflected radiation, defined as $R_{COMBINED} = R_{LAMP} + R_{PHOSPHOR}$, was measured. This measurement can be considered representative of the radiation to which a microbiological sample would be exposed.

The primary KrCl emission line at 222 nm is reflected from the surface. Compared to a neutral surface (i.e., raw quartz), this reflection is increased by 80% with the SP phosphor and by a factor 40% with the SSR phosphor [Fig. 9(a)].

On the basis of reflection measurements, an analysis of the $R_{COMBINED}$ spectrum in the 200–400 nm UV range indicates that the incorporation of luminophores results in a more balanced distribution of emissions between the UVC and UVB spectral regions [Fig. 10(a)]. Without a phosphor, where R_{LAMP} is only reflected off a raw quartz surface, 83% of the UV emissions are concentrated in the UVC range, primarily dominated by the KrCl line at 222 nm (65%), whereas only 17% are distributed between the UVB and UVA ranges. The addition of a phosphor not only enhances the reflection of the KrCl line but also significantly increases emissions in the 225–400 nm range [Fig. 10(b)]. Specifically, the SP phosphor increases UVB emissions by a factor of 12.5 and UVA emissions by a factor of 7.4, whereas the SSR phosphor increases UVB emissions by a factor of 7.6 and UVA emissions by a factor of 7.6.

A comparison between the SP and SSR powders highlights that the SP phosphor achieves a greater enhancement of emissions across the entire UV range, making it the

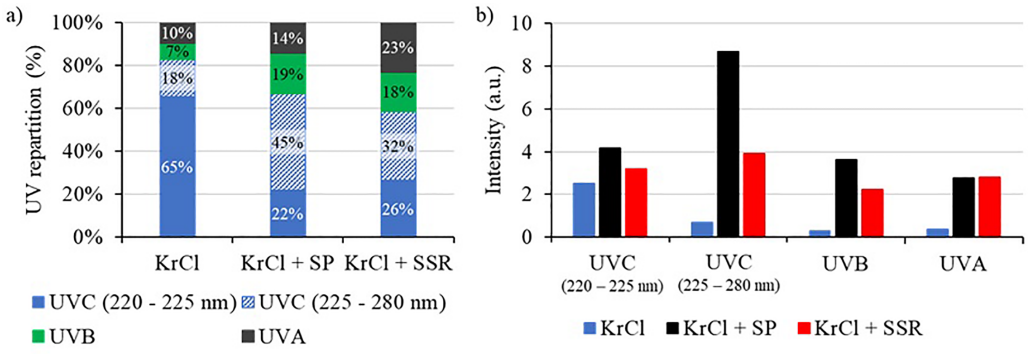

FIG. 10: (a) Repartition and (b) intensity of emissions in UVC (220–225 nm), UVC (225–280 nm), UVB, and UVA ranges for the KrCl excimer lamp alone, and the KrCl excimer lamp combined with SP (KrCl+SP) and with SSR phosphors (KrCl+SSR), measured in reflection

more effective of the two from a physics point of view. The microbiological results will confirm this conclusion.

C. Decontamination Efficiency

1. Bacteria Inactivation Efficacy

Figure 11 shows the survival curves of *E. coli* [Fig. 11(a)] and *S. aureus* [Fig. 11(b)] after the contaminated samples were exposed to a conventional mercury lamp (OSRAM PURITEC HNS 15W G13), the KrCl lamp and the KrCl lamp combined with one of the phosphors [Fig. 11(c)]. The mercury lamp operates at 15 W, while the KrCl lamp operates at 20 W. Despite the higher power of the KrCl source, the irradiance delivered to a surface at the same distance is significantly greater for the mercury lamp. To enable a meaningful comparison between the two sources, the distance to the sample was adjusted such that the irradiance—and consequently the UV dose—was equivalent for both lamps. The exposure durations were 5, 10, 20, 30, and 60 s, corresponding to a dose of 2.9, 5.8, 11.6, 17.4, and 34.8 mJ/cm² for the two lamps.

Under our experimental conditions, the comparative analysis of the decontamination efficiency of the KrCl excimer lamp (black circle) and the mercury lamp (black diamond) demonstrated the superior performance of the mercury lamp. To achieve a two-log reduction in bacterial load, the KrCl lamp required a dose 2.4 times higher than that of the mercury lamp for *E. coli* and 12.4 times higher for *S. aureus*. However, the integration of the KrCl lamp with either of the two phosphors significantly enhanced its

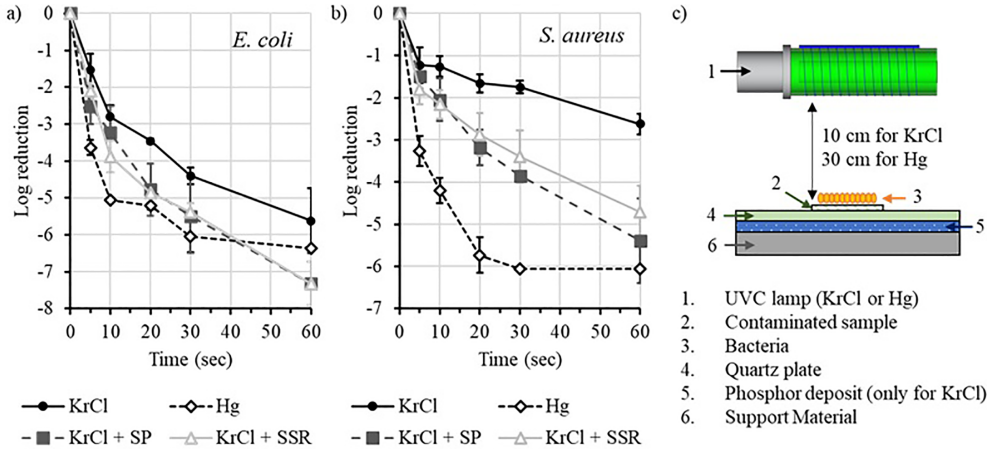

FIG. 11: Survival curve of (a) *E. coli* and (b) *S. aureus* after being exposed to the KrCl excimer lamp alone (black circle) or combined with the SP (gray square) and SSR (gray triangle) phosphorus, and a conventional Hg lamp (black diamond). (c) Experimental set-up for microbiological tests.

biocidal efficiency. After 30 s of treatment, the incorporation of phosphors resulted in an additional one-log reduction in *E. coli* and a 1.8-log reduction in *S. aureus.*

Ultraviolet devices emitting UVC (200–280 nm), UVB (280–320 nm), and UVA (320–400 nm) irradiation, such as the low-pressure mercury lamp (LPHg), excimer lamp, and UV light-emitting diodes (LEDs) have been widely used for disinfection of water, air, and surfaces. Because of their low absorption, UVA decontamination is not very effective unless treatment time and irradiation dose are considerably increased to obtain a result comparable to UVC or UVB.[46–48] The variability of the results concerning UVC and UVB decontamination, which are sometimes contradictory, makes it impossible to state that one irradiation wavelength is better than another. Jing et al.[49] observed that exposure to the 222 nm light demonstrated higher inactivation efficacy than the Hg lamp for *Pseudomonas aeruginosa*, *Bacillus subtilis*, and *Pantoea spp*. However, this wavelength was less effective against *Mycobacterium fortuitum* and *Stenotrophomonas spp*.

Similarly, Rattanakul and Oguma[50] found that UV-LEDs emitting at 265 nm, and 280 nm were more effective in inactivating *P. aeruginosa*, *Legionella pneumophila*, and *B. subtilis* spores compared to conventional LPHg. These UV-LEDs were also equally effective as LPHg for *E. coli* inactivation. Li et al. [51] confirmed that UV-LEDs at 265 nm outperformed both 280 nm LEDs and mercury lamps for inactivating *E. coli*.

For bacteria and mold spores, Clauß[52] reported that the UV fluences required with KrCl excimer lamps were lower than those for mercury lamps to inactivate *Deinococcus radiodurans*, spores of *Bacillus cereus*, and *Trichonius griseus*, and molds like *Aspergillus niger* and *Penicillium expansum*. However, mercury lamps were more efficient at killing vegetative bacteria, such as *B. cereus*, *A. nicotinovorans*, *S. aureus*, and *P. aeruginosa*, as well as spores of *Streptomyces griseus* and *Clostridium pasteurianum*. Clauß and Grotjohann[53] suggested that microorganisms with higher UV resistance and more effective repair mechanisms were better inactivated by 222 nm excimer lamps.

Kang et al.[54] also demonstrated that KrCl excilamps had a stronger bactericidal effect than mercury lamps on microorganisms suspended in PBS, including *S. aureus*, *Listeria monocytogenes*, *Salmonella typhimurium*, and *E. coli* O157:H7. Among these microorganisms, *S. aureus* exhibited the highest resistance to UV irradiation, followed by *L. monocytogenes*, *S. typhimurium*, and *E. coli* O157:H7. Additionally, differences in UV-C sensitivity were observed between strains of the same species, such as *E. coli* or *L. monocytogenes*.[55–57] This disparity in results can be attributed to the fact that each UV wavelength operates through distinct and complementary mechanisms, determined by differences in biomolecular absorption. The maximum absorption wavelengths of major amino acids are all < 240 nm,[58,59] whereas nucleic acids (DNA and RNA) exhibit maximum UV absorption at 260 nm and proteins show prominent absorption peaks of ~ 280 nm.[60,61]

Upon exposure to UV light at wavelengths such as 254 or 265 nm, nucleic acids undergo damage primarily through the formation of pyrimidine cyclobutane dimers, pyrimidine (6-4) photoproducts, and their Dewar isomers,[49,62] Although this type of DNA damage occurs to a lesser extent at 222 nm, it still disrupts replication and gene

expression, ultimately leading to cell death.[63] In addition to direct DNA damage, UV radiation induces the generation of reactive oxygen species (ROS), including singlet oxygen ($^1O_2$), hydrogen peroxide (H_2O_2), and hydroxyl radicals (OH•), particularly in photosensitive compounds both inside and outside cells. These ROS primarily target major aromatic amino acids, such as phenylalanine, tryptophan, and tyrosine.[54] The accumulation of intracellular ROS leads to oxidative damage of membrane proteins, enzymes, and lipids, compromising membrane integrity and resulting in cell death.[49] Notably, while DNA dimer formation is a common mechanism of UV-induced damage, protein photodegradation, enzyme inactivation, and lipid peroxidation occur more efficiently with a 222 nm KrCl excimer lamp than with a conventional 254 nm mercury lamp.[64,65]

Figure 12 shows SEM images of *E. coli* and *S. aureus* bacteria treated under our experimental conditions. Lesions appear in the membrane of *E. coli* after exposure to the KrCl lamp alone (222 nm) or in combination with the SSR phosphor, but no change was observed at 254 nm. The structure of *S. aureus* remained intact at all wavelengths. This is probably due to differences in membrane structures between Gram-negative and Gram-positive bacteria, with a thicker peptidoglycan layer in Gram-positive bacteria such as *S. aureus*.[66]

Under our experimental conditions, the addition of a luminophore increases the number of log reductions for a given time. We know that, at wavelengths shorter than 240 nm, the germicidal mechanism is mostly protein degradation, whereas at wavelengths higher than 240 nm, nucleic acids are damaged. We suggest that the improvement in biocidal efficacy in the presence of luminophore is a combination of these phenomena.

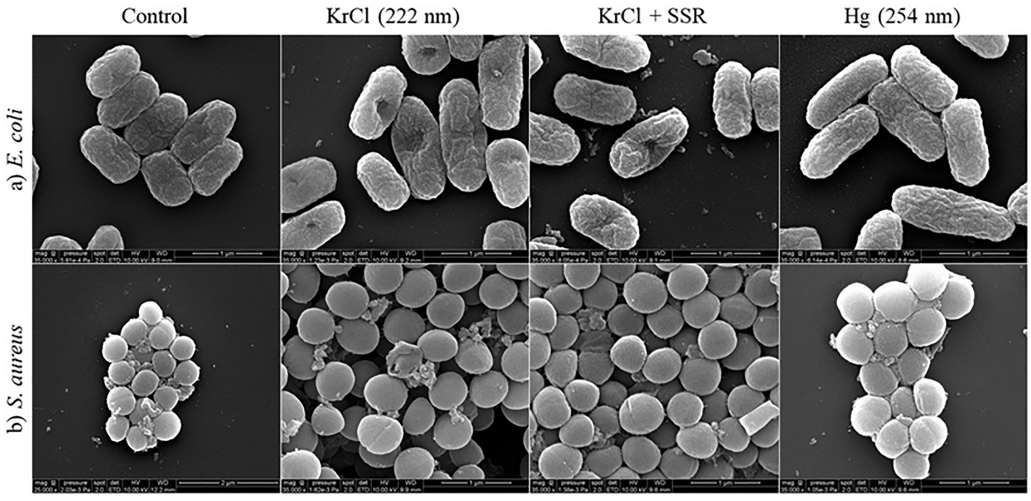

FIG. 12: SEM images of (a) *E. coli* and (b) *S. aureus* after being exposed to the KrCl excimer lamp alone, combined with the SSR phosphor and a conventional Hg lamp

2. Virucidal Decontamination

Figure 13 shows fluorescence images of the HAdV5 virus after being kept in the dark [Fig. 13(a)], irradiated with the KrCl lamp in the absence of phosphor [Fig. 13(b)] or with the SSR phosphor [Fig. 13(c)]. The dose received by the lamp was fixed at 34.8 mJ/cm² corresponding to a distance of 10 cm between the sample and the lamp; there was a treatment time of 60 s and a power injected to the lamp of 20 W.

In contrast to the control group, which shows a significant number of fluorescent nuclei, only a few nuclei are visible after viral exposure to the KrCl lamp (R_{LAMP}), and none are detected following exposure to the KrCl lamp combined with SSR phosphor ($R_{LAMP} + R_{PHOSPHOR}$). This results in a viral load reduction of 97.26% with the KrCl lamp alone, and 99.77% reduction when combined with the SSR luminophore [Fig. 13(d)].

To understand how the UV inactivates viruses, it is necessary to give a brief description of these pathogens. Viruses are lifeforms with a genome (DNA or RNA) wrapped in a protein structure called a nucleocapsid, which may be surrounded by a lipid membrane. The surface structures of viruses enable them to bind to specific receptors on host cells, which are made of proteins, carbohydrates, and/or lipids. Once attached, the viral genome is released into the cell either through direct fusion or receptor-mediated endocytosis.[67]

Similar to bacteria, viruses can be affected by various lethal mechanisms. The genetic material in the viral capsid strongly absorbs UV radiation close to 254 nm,[68,69] while the proteins are minor absorbers but still involved in virus inactivation, especially at a lower wavelength.[70,71] UV radiation can destabilize the capsid, degrade it, and form covalent bonds between proteins and RNA,[72] rendering the virus noninfectious.

The virucidal effect of UVs have been extensively documented across various microorganisms. Beck et al.[73] obtained on MS2 coliphage two-log inactivation at 30.3 mJ/cm² (260 nm), 38.5 mJ/cm² (280 nm), and 32.8 mJ/cm² (254 nm). They also achieved on HAdV2 3-log inactivation at 64–68 mJ/cm² and four-log at 122 mJ/cm² (260 nm), 89 mJ/cm² (280 nm), 105 mJ/cm² (260–280 nm). The mercury lamp was still the best with a dose required of 26 and 38 mJ/cm² for three- and four-log reductions, respectively.

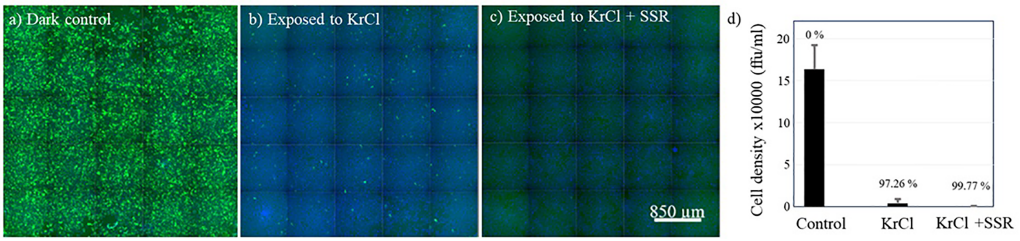

FIG. 13: (a) Virus sample not irradiated (control), (b) virus sample after 60 s of irradiation under the KrCl lamp, (c) virus sample after 60 s of irradiation under the KrCl lamp in combination with phosphore, and (d) quantification of disinfection efficiency under the tested conditions (a–c)

Welch et al.[74] show for the first time that far-UVC efficiently inactivates airborne aerosolized viruses, with a very low dose of 2 mJ/cm^2 of 222-nm light inactivating > 95% of aerosolized H1N1 influenza virus. Tarasenko et al.[41] observed higher sensitivity of MS2 bacteriophage to UV radiation of XeBr excilamp (280 nm) than the LP Hg-lamp at the same UV doses (4.5 mJ/cm^2) compared to control. Ma et al.[75] also highlighted that KrCl excimer lamps outperformed mercury lamps and UV-LEDs emitting at 270 and 282 nm for inactivating viruses such as SARS-CoV-2 murine hepatitis virus and bacteriophage Phi6.

IV. CONCLUSION

This study highlighted the spectral characteristics and microbiological performance of KrCl excimer lamps, in combination with two luminophores, produced by SP and SSR, respectively. The results obtained show several distinct advantages of 222 nm excimer lamps in combination with phosphor, including their ability to provide concentrated UV-C emission, rapid start-up, and independence from temperature conditions.

Spectral characterization reveals that the SP luminophore outperforms SSR in terms of intensity and balance in emission distribution between the UV-C, UV-B, and UV-A ranges. The addition of luminophores significantly improves the germicidal efficacy of KrCl lamps, with increased reductions in bacterial and viral load. This improvement is explained by the complementary mechanisms of biomolecular absorption, where wavelengths of < 240 nm promote protein degradation and those of > 240 nm cause nucleic acid damage. Nevertheless, under our experimental conditions, the mercury lamp exhibited superior efficacy compared to the KrCl+SP/SSR combinations in inactivating *S. aureus*. This result is likely due to the structural properties of Gram-positive bacteria, because its thick, peptidoglycan-rich cell wall provides increased resistance to shorter wavelengths (< 240 nm).

Considering the surface disinfection, the incorporation of SP and SSR luminophores serves not only to augment the germicidal efficacy of excimer lamps but also to diversify the range of wavelengths available. This expansion could allow for broader applications. These advancements, along with the inherent benefits of excimer lamps, make them promising alternatives to mercury lamps, particularly in situations that require rapid, efficient, and potentially more environmentally friendly disinfection. Finally, these results open up interesting prospects for optimizing surface disinfection, while suggesting that future studies could further explore the effect of operating parameters and host matrices on luminophore performance and excimer lamp efficacy.

ACKNOWLEDGMENTS

This research was funded by the French National Association for Research and Technology (ANRT, CIFRE 2020 – 0273). We thank Dr. Vereslst for his involvement in the production and characterization of the luminophores, and Dr. Bohsle for

his contribution to the electrical characterization of the KrCl lamp. We also thank Dr. Gallardo and Dr. Macheteau from Neovirtech for their expertise on viruses.

AUTHOR CONTRIBUTIONS

A.B.: investigation, data curation, formal analysis, writing – original draft (supporting);. C.M.: methodology, formal analysis, writing and reviewing; I.C.: investigation, data curation, formal analysis, writing, and reviewing; F.P.S.: methodology and reviewing; S.A.: conceptualization, supervision, reviewing and funding acquisition; Ph.G.: conceptualization, methodology, supervision, and funding acquisition; and T.M.: conceptualization, methodology, data curation, formal analysis, investigation, writing – original draft (lead), reviewing, and editing.

REFERENCES

1. Miettinen H, Aarnisalo K, Salo S, Sjöberg AM. Evaluation of surface contamination and the presence of listeria monocytogenes in fish processing factories. J Food Prot. 2001;64(5):635–9.
2. Gutiérrez D, Delgado S, Vázquez-Sánchez D, Martínez B, Cabo ML, Rodríguez A, Herrera JJ, García P. Incidence of staphylococcus aureus and analysis of associated bacterial communities on food industry surfaces. Appl Environ Microbiol. 2012;78(24):8547–54.
3. Lehto M, Kuisma R, Määttä J, Kymäläinen HR, Mäki M. Hygienic level and surface contamination in fresh-cut vegetable production plants. Food Control. 2011;22(3-4):469–75.
4. Barker J, Stevens D, Bloomfield SF. Spread and prevention of some common viral infections in community facilities and domestic homes. J Appl Microbiol. 2001;91:7–21.
5. Russotto V, Cortegiani A, Raineri SM, Giarratano A. Bacterial contamination of inanimate surfaces and equipment in the intensive care unit. J Intensive Care. 2015;3(54).
6. Dancer SJ. Controlling hospital-acquired infection: Focus on the role of the environment and new technologies for decontamination. Clin Microbiol Rev. 2014;27(4):665–90.
7. Kramer A, Schwebke I, Kampf G. How long do nosocomial pathogens persist on inanimate surfaces? A systematic review. BMC Infect Dis. 2006;6:130.
8. Carraturo F, Del Giudice C, Morelli M, Cerullo V, Libralato G, Galdiero E, Guida M. Persistence of SARS-CoV-2 in the environment and COVID-19 transmission risk from environmental matrices and surfaces. Environ Pollut. 2020;265.
9. Wißmann JE, Kirchhoff L, Brüggemann Y, Todt D, Steinmann J, Steinmann E. Persistence of pathogens on inanimate surfaces: A narrative review. Microorganisms. 2021;9(2):1–37.
10. Boyce JM. Modern technologies for improving cleaning and disinfection of environmental surfaces in hospitals. Antimicrob Resist Infect Control. 2016;5(10).
11. Russell AD. Similarities and differences in the responses of microorganisms to biocides. J Antimicrob Chemother. 2003;52(5):750–63.
12. Dancer SJ. The role of environmental cleaning in the control of hospital-acquired infection. J Hosp Infect. 2009;73(4):378–85.
13. Dancer SJ. Hospital cleaning in the 21st century. Eur J Clin Microbiol Infect Dis. 2011;30(12):1473–81.
14. Bridier A, Briandet R, Thomas V, Dubois-Brissonnet F. Comparative biocidal activity of peracetic acid, benzalkonium chloride and ortho-phthalaldehyde on 77 bacterial strains. J Hosp Infect. 2011;78(3):208–13.
15. Vickery K, Deva A, Jacombs A, Allan J, Valente P, Gosbell IB. Presence of biofilm containing viable multiresistant organisms despite terminal cleaning on clinical surfaces in an intensive care unit. J Hosp Infect. 2012;80(1):52–5.

16. Hota B, Blom DW, Lyle EA, Weinstein RA, Hayden MK. Interventional evaluation of environmental contamination by vancomycin-resistant enterococci: Failure of personnel, product, or procedure? J Hosp Infect. 2009;71(2):123–31.
17. Courti I, Muja C, Maho T, Sainct FP, Guillot P. Degradation of bacterial antibiotic resistance genes during exposure to non-thermal atmospheric pressure plasma. Antibiotics. 2022;11(6):747.
18. Hegstad K, Langsrud S, Lunestad BT, Scheie AA, Sunde M, Yazdankhah SP. Does the wide use of quaternary ammonium compounds enhance the selection and spread of antimicrobial resistance and thus threaten our health? Microb Drug Resist. 2010;16(2):91–104.
19. Otto C, Zahn S, Rost F, Zahn P, Jaros D, Rohm H. Physical methods for cleaning and disinfection of surfaces. Food Eng Rev. 2011;3(3-4):171–88.
20. Fan X, Huang R, Chen H. Application of ultraviolet C technology for surface decontamination of fresh produce. Trends Food Sci Technol. 2017;70:9–19.
21. Naito K, Sawadaishi K, Kawasaki M. Photobiochemical mechanisms of biomolecules relevant to germicidal ultraviolet irradiation at 222 and 254 nm. Sci Rep. 2022;12(1).
22. Chatterley C, Linden K. Demonstration and evaluation of germicidal UV-LEDs for point-of-use water disinfection. J Water Health. 2010;8(3):479–86.
23. Crawford MH, Banas MA, Ross MP, Ruby DS, Nelson JS, Boucher R, Allerman AA. Final LDRD Report: Ultraviolet water purification systems for rural environments and mobile applications. 2005. Report No. SAND2005-7245. Contract No: DE-AC04-94AL85000.
24. Ikehata H, Mori T, Yamamoto M. In vivo spectrum of UVC-induced mutation in mouse skin epidermis may reflect the cytosine deamination propensity of cyclobutane pyrimidine dimers. Photochem Photobiol. 2015;91(6):1488–96.
25. Cadet J, Sage E, Douki T. Ultraviolet radiation-mediated damage to cellular DNA. Mutat Res. 2005;571(1-2 SPEC. ISS.):3–17.
26. Zhang JY, Boyd IW. Lifetime investigation of excimer UV sources. Appl Surf Sci. 2000;168:296–9.
27. Kogelschatz U. Excimer lamps: History, discharge physics, and industrial applications. In: Tarasenko VF, Mayer GV, Petrash GG, editors. Atomic and molecular pulsed lasers. V. Bellingham: SPIE; 2004. p. 272–86.
28. Lomaev MI, Sosnin EA, Tarasenko VF. Excilamps and their applications. Prog Quantum Electron. 2012;36(1):51–97.
29. Sugihara K, Kaidzu S, Sasaki M, Ichioka S, Sano I, Hara K, Tanito M. Ocular safety of 222-nm far-ultraviolet-c full-room germicidal irradiation: A 36-month clinical observation. Photochem Photobiol. 2024:1–7.
30. Buonanno M, Welch D, Brenner DJ. Exposure of human skin models to KrCl excimer lamps: The impact of optical filtering. Photochem Photobiol. 2021;97(3):517–23.
31. Masoud NM, Murnick DE. High efficiency fluorescent excimer lamps: An alternative to mercury based UVC lamps. Rev Sci Instrum. 2013;84(12):123108.
32. Caiut JMA, Lechevallier S, Dexpert-Ghys J, Caillier B, Guillot P. UVC emitting phosphors obtained by spray pyrolysis. J Lumin. 2011;131(4):628–32.
33. Caillier B, Caiut JMA, Muja C, Demoucron J, Mauricot R, Dexpert-Ghys J, Guillot P. Decontamination efficiency of a DBD lamp containing an UV-C emitting phosphor. Photochem Photobiol. 2015;91(3):526–32.
34. Masjoudi M, Mohseni M, Bolton JR. Sensitivity of bacteria, protozoa, viruses, and other microorganisms to ultraviolet radiation. J Res Natl Inst Stand Technol. 2021;126:126021.
35. Allix S, Maho T, Guillot P. Système de décontamination par double rayonnements UVC. France; FR2314652, 2024.
36. Al-Qahtani SD, Alzahrani SO, Snari RM, Al-Ahmed ZA, Alkhamis K, Alhasani M, El-Metwaly NM. Preparation of photoluminescent and photochromic smart glass window using sol-gel technique and lanthanides-activated aluminate phosphor. Ceram Int. 2022;48(12):17489–98.
37. Lomaev MI, Skakun VS, Sosnin EA, Tarasenko VF, Shitts DV, Erofeev MV. Excilamps: Efficient sources of spontaneous UV and VUV radiation. Phys Usp. 2003;46(2):193–209.

38. Zhang JY, Boyd IW. Efficient excimer ultraviolet sources from a dielectric barrier discharge in rare-gas/halogen mixtures. J Appl Phys. 1996;80(2):633–8.
39. Sosnin EA, Oppenländer T, Tarasenko VF. Applications of capacitive and barrier discharge excilamps in photoscience. J Photochem Photobiol C. 2006;7(4):145–63.
40. Lomaev MI, Tarasenko VF, Tkachev AN, Shitts DV, Yakovlenko SI. Formation of coniform microdischarges in KrCl and XeCl excimer lamps. Tech Phys. 2004;49(6):790–4.
41. Tarasenko VF, Sosnin EA, Zhdanova OS, Krasnozhenov EP. Applications of excilamps in microbiological and medical investigations. In: Machala Z, Hensel K, Akishev Y, editors. Plasma for biodecontamination, medicine and food security. New York: Springer; 2012. p. 251–63.
42. Srivastava AM. Aspects of Pr^{3+} luminescence in solids. J Lumin. 2016;169:445–9.
43. Srivastava AM, Jennings M, Collins J. The interconfigurational ($4f^15d^1 \rightarrow 4f^2$) luminescence of Pr^{3+} in $LuPO_4$, $K_3Lu(PO_4)^2$ and $LiLuSiO_4$. Opt Mater (Amst). 2012;34(8):1347–52.
44. Srivastava AM, Setlur AA, Comanzo HA, Beers WW, Happek U, Schmidt P. The influence of the Pr^{3+} $4f^15d^1$ configuration on the $1S_0$ emission efficiency and lifetime in $LaPO_4$. Opt Mater. 2011;33(3): 292–8.
45. Srivastava AM, Setlur AA, Comanzo HA, Hannah ME, Schmidt PA, Happek U. Luminescence from the Pr^{3+} $4f^15d^1$ and $1S_0$ states in $LiLaP_4O_{12}$. J Lumin. 2009;129(2):126–9.
46. Song K, Mohseni M, Taghipour F. Application of ultraviolet light-emitting diodes (UV-LEDs) for water disinfection: A review. Water Res. 2016;94:341–9.
47. Chevremont AC, Farnet AM, Coulomb B, Boudenne JL. Effect of coupled UV-A and UV-C LEDs on both microbiological and chemical pollution of urban wastewaters. Sci Total Environ. 2012;426:304–10.
48. Oguma K, Kita R, Sakai H, Murakami M, Takizawa S. Application of UV light emitting diodes to batch and flow-through water disinfection systems. Desalination. 2013;328:24–30.
49. Jing Z, Lu Z, Santoro D, Zhao Z, Huang Y, Ke Y, Wang X, Sun W. Which UV wavelength is the most effective for chlorine-resistant bacteria in terms of the impact of activity, cell membrane and DNA? Chem Eng J. 2022;447.
50. Rattanakul S, Oguma K. Inactivation kinetics and efficiencies of UV-LEDs against Pseudomonas aeruginosa, Legionella pneumophila, and surrogate microorganisms. Water Res. 2018;130:31–7.
51. Li GQ, Wang WL, Huo ZY, Lu Y, Hu HY. Comparison of UV-LED and low pressure UV for water disinfection: Photoreactivation and dark repair of Escherichia coli. Water Res. 2017;126:134–43.
52. Clauß M. Higher effectiveness of photoinactivation of bacterial spores, UV resistant vegetative bacteria and mold spores with 222 nm compared to 254 nm wavelength. Acta Hydrochim Hydrobiol. 2006;34(6):525–32.
53. Clauß M, Grotjohann N. Effective photoinactivation of alpha-amylase, catalase and urease at 222 nm emitted by an KrCl-excimer lamp. Clean. 2008;36(9):754–9.
54. Kang JW, Kim SS, Kang DH. Inactivation dynamics of 222 nm krypton-chlorine excilamp irradiation on gram-positive and gram-negative foodborne pathogenic bacteria. Food Res Int. 2018;109:325–33.
55. Quek PH, Hu J. Indicators for photoreactivation and dark repair studies following ultraviolet disinfection. J Ind Microbiol Biotechnol. 2008;35(6):533–41.
56. Gayán E, Serrano MJ, Pagán R, Álvarez I, Condón S. Environmental and biological factors influencing the UV-C resistance of Listeria monocytogenes. Food Microbiol. 2015;46:246–53.
57. Yan R, Liu Y, Gurtler JB, Killinger K, Fan X. Sensitivity of pathogenic and attenuated E. coli O157:H7 strains to ultraviolet-C light as assessed by conventional plating methods and ethidium monoazide-PCR. J Food Saf. 2017;37(4):e12346.
58. Beaven GH, Holiday ER. Ultraviolet absorption spectra of proteins and amino acids. Adv Protein Chem. 1952;7:319–86.
59. Wetlaufer DB. Ultraviolet spectra of proteins and amino acids. Adv Protein Chem. 1963;17:303–90.
60. Seltsam A, Müller TH. UVC irradiation for pathogen reduction of platelet concentrates and plasma. Transfus Med Hemotherapy. 2011;38(1):43–54.

61. Nishigori C, Yamano N, Kunisada M, Nishiaki-Sawada A, Ohashi H, Igarashi T. Biological impact of shorter wavelength ultraviolet radiation-c. Photochem Photobiol. 2023;99(2):335–43.
62. Coohill TP, Sagripanti JL. Overview of the inactivation by 254 nm ultraviolet radiation of bacteria with particular relevance to biodefense. Photochem Photobiol. 2008;84(5):1084–90.
63. Kim DK, Kim SJ, Kang DH. Bactericidal effect of 266 to 279 nm wavelength UVC-LEDs for inactivation of gram positive and gram negative foodborne pathogenic bacteria and yeasts. Food Res Int. 2017;97:280–7.
64. Clauß M. Higher effectiveness of photoinactivation of bacterial spores, UV resistant vegetative bacteria and mold spores with 222 nm compared to 254 nm wavelength. Acta Hydrochim Hydrobiol. 2006;34(6):525–32.
65. Ha JW, Lee JI, Kang DH. Application of a 222-nm krypton-chlorine excilamp to control foodborne pathogens on sliced cheese surfaces and characterization of the bactericidal mechanisms. Int J Food Microbiol. 2017;243:96–102.
66. Beauchamp S, Lacroix M. Resistance of the genome of Escherichia coli and Listeria monocytogenes to irradiation evaluated by the induction of cyclobutane pyrimidine dimers and 6-4 photoproducts using gamma and UV-C radiations. Radiat Phys Chem. 2012;81(8):1193–7.
67. Gómez-López VM, Jubinville E, Rodríguez-López MI, Trudel-Ferland M, Bouchard S, Jean J. Inactivation of foodborne viruses by UV light: A review. Foods. 2021;10(3141).
68. Lytle CD, Sagripanti JL. Predicted inactivation of viruses of relevance to biodefense by solar radiation. J Virol. 2005;79(22):14244–52.
69. Kong J, Lu Y, Ren Y, Chen Z, Chen M. The virus removal in UV irradiation, ozonation and chlorination. Water Cycle. 2021;2:23–31.
70. Eischeid AC, Linden KG. Molecular indications of protein damage in adenoviruses after UV disinfection. Appl Environ Microbiol. 2011;77(3):1145–7.
71. Sosnin EA, Zhdanova OS. Viricidal and bactericidal exciplex barrier-discharge lamps. Quantum Elec. 2020;50(10):984–8.
72. Miller RL, Plagemann PGW. Effect of ultraviolet light on mengovirus: Formation of uracil dimers, instability and degradation of capsid, and covalent linkage of protein to viral RNA. J Virol. 1974;13(3):729–39.
73. Beck SE, Ryu H, Boczek LA, Cashdollar JL, Jeanis KM, Rosenblum JS, Lawal OR, Linden KG. Evaluating UV-C LED disinfection performance and investigating potential dual-wavelength synergy. Water Res. 2017;109:207–16.
74. Welch D, Buonanno M, Grilj V, Shuryak I, Crickmore C, Bigelow AW, Randers-Pehrson G, Johnson GW, Brenner DJ. Far-UVC light: A new tool to control the spread of airborne-mediated microbial diseases. Sci Rep. 2018;8(1):2752.
75. Ma B, Gundy PM, Gerba CP, Sobsey MD, Linden KG. UV Inactivation of SARS-CoV-2 across the UVC spectrum: KrCl* excimer, mercury-vapor, and light-emitting-diode (LED) sources. Appl Environ Microbiol. 2021;87(22):e01532-21.